Spontaneous magnetic order and spin and charge entanglement of a coupled spin-electron model on a decorated square lattice composed from trigonal bipyramids

Lucia Gálisová [1,*] and Jozef Strečka [2]

[1] *Institute of Manufacturing Management, Faculty of Manufacturing Technologies with the seat in Prešov, Technical University of Košice, Bayerova 1, 080 01 Prešov, Slovak Republic*

[2] *Department of Theoretical Physics and Astrophysics, Faculty of Science, P. J. Šafárik University, Park Angelinum 9, 040 01, Košice, Slovak Republic*

(Received 1 July 2021; revised 8 September 2021; accepted 13 September 2021; published 21 September 2021)

A coupled spin-electron model on a decorated square lattice formed by interconnected trigonal bipyramids is exactly solved by imposing two mobile electrons per each triangular plaquette with the help of a generalized decoration-iteration transformation, which establishes a precise mapping correspondence with the effective Ising model on a square lattice with temperature-dependent interaction. The investigated spin-electron model exhibits two different macroscopically degenerate ground states. The residual entropy of the first ground state, which shows a spontaneous ferromagnetic or ferrimagnetic long-range order depending on character of the exchange coupling, arises from chiral degrees of freedom of the mobile electrons. In contrast, the second ground state is disordered due to a kinetically driven frustration of the localized Ising spins triggered by the hopping term of the mobile electrons. The outstanding reentrant phase transitions connected with temperature induced formation of the spontaneous ferromagnetic or ferrimagnetic order can be found if the spin-electron model is driven sufficiently close to the ground-state phase boundary, but the disordered frustrated phase is the respective ground state. It is verified that the bipartite fermionic entanglement between two mobile electrons within the spontaneously ordered ferromagnetic or ferrimagnetic phase predominantly comes from their charge degrees of freedom, while the one within the disordered frustrated phase comes from both charge and spin degrees of freedom of these particles.

DOI: 10.1103/PhysRevB.104.104420

I. INTRODUCTION

Quantum entanglement currently attracts a renewed interest, because it is considered as primary resource for a development of novel quantum technologies, quantum computers, and quantum information science [1]. However, the most limiting obstacle preventing progress in this cutting-edge research field is a lack of suitable physical realization of a quantum computer, which would serve as a hardware for performing computational tasks with the help of efficient quantum algorithms [2,3]. Although there are a lot of promising candidates for a physical realization of quantum computers such as photonic qubits [4], ionic traps [5], superconducting circuits [6], nuclear spins [7], topological qubits [8], and quantum dots [9], none of these physical systems still satisfy all DiVincenzo criteria such as scalability, easy initialization, accurate quantum gate operation, low quantum decoherence, and reliable readout [10,11].

It should be pointed out, moreover, that the most efficient quantum algorithms cannot be realized without implementation of quantum-mechanically entangled qubits [3]. Electron spin systems afford another promising and tunable platform for a physical realization of entangled qubits with regard to a two-level character of the electron spin [12]. A loss of quantum information due to a quantum decoherence is, however, the most principal limiting factor for exploitation of the electron spin systems for quantum computation [13]. From this point of view, it appears worthwhile to investigate how robust is the quantum entanglement of electron spin systems with respect to rising temperature and magnetic field. While the robustness of bipartite entanglement of quantum spin systems is well understood nowadays, the fermionic entanglement of correlated electron systems is still far from being fully understood yet [14].

The complexity of strongly correlated electron systems usually prohibits their rigorous solution and hence, one should resort to some numerical or approximate analytical treatment [15]. From this perspective, exact results for coupled spin-electron systems are very rare and highly desirable, because they allow comprehensive analysis of the fermionic entanglement without any artifact stemming from some approximation. If a quantum-mechanical hopping of the mobile electrons is restricted to a few lattice sites and they are merely coupled indirectly through the exchange interaction with localized Ising spins, then one may adapt the concept of generalized mapping transformations in order to derive the relevant exact solutions [16–19]. As a matter of fact, this concept has been recently adapted for an exact investigation of a coupled spin-electron diamond chain [20–26], two-leg ladder [27–30], trimerized chain [31–33], double-tetrahedral chain [34–39], or doubly decorated square lattice [40–50].

*galisova.lucia@gmail.com

In the present paper we will propose and exactly solve a coupled spin-electron model on a decorated square lattice composed by interconnected trigonal bipyramids, which contain two mobile electrons within each triangular plaquette. Our main goal is to examine a mutual interplay between a possible spontaneous long-range order and a fermionic entanglement [51,52]. Although the quantity concurrence has been originally suggested as a suitable measure of the bipartite entanglement only for two-qubit systems [53,54], it was recently recognized that the concept of fermionic concurrence can be elaborated much more generally in restricted Hilbert subspaces. The fermionic concurrences calculated in this way may thus additionally provide a partial information on a mutual interplay/competition of the charge and spin entanglement [55,56]. Another intriguing issue is whether the charge and spin entanglement compete with a spontaneous magnetic long-range order or they may concurrently occur together with a spontaneous magnetic ordering.

Besides the purely academic interest, our theoretical investigation of a coupled spin-electron model on a decorated square lattice formed by interconnected trigonal bipyramids is motivated by the copper-based magnetic compound $Cu_3Mo_2O_9$, which represents the experimental realization of the analogous one-dimensional (1D) double-tetrahedral spin chain [57–59]. Moreover, there exist a few higher-dimensional geometrically frustrated magnetic compounds such as cobaltates $R\mathrm{BaCo_4O_7}$ (R is a rare-earth ion) [60] and anion-radical salts $(\mathrm{MDABCO}^+)(\mathrm{C}_{60}^{\bullet -})$ (MDABCO^+ labels N-methyldiazabicyclooctanium cation and $\mathrm{C}_{60}^{\bullet -}$ is radical anion) [61], in which one can clearly identify interconnected trigonal bipyramidal units. Although the latter two magnetic compounds do not represent a precise experimental realization of the magnetic structure proposed in the present paper, we hope that a targeted design of the magnetic material with a magnetic structure consisting of interconnected trigonal bipyramids is feasible. The targeted chemical synthesis involving highly anisotropic spin carriers such Dy^{3+} or Co^{2+} magnetic ions and anion-radical salts could possibly afford desired coupled spin-electron system composed of the localized Ising spins and mobile electrons, whereby the findings presented in this paper could serve as a strong motivation for achieving this goal.

The outline of the paper is as follows. In Sec. II we will describe in detail the investigated spin-electron model on a decorated square lattice composed from interconnected trigonal bipyramids and then, the most important steps of an exact mapping method will be clarified. In Sec. III we will discuss the most interesting results for the ground state, critical behavior and temperature dependencies of basic thermodynamic quantities (magnetization, entropy, specific heat). The section also includes a detailed discussion about the fermionic entanglement and its three contributions: charge, zero-spin, and single spin concurrences. Finally, the paper ends up with a brief summary of the most interesting findings in Sec. IV.

II. MODEL AND ITS EXACT SOLUTION

Let us consider a coupled spin-electron model on a decorated square lattice formed by corner-sharing trigonal bipyramids, which involves the localized Ising spins at nodal sites of a square lattice and two mobile electrons delocalized over each decorating triangular plaquette oriented perpendicularly to unit axes of a square lattice (see Fig. 1 for a schematic illustration). Our attention will be focused on a special case, which assumes that a quantum-mechanical hopping of the mobile electrons is restricted to a given decorating triangular plaquette. In other words, the electron passing between different trigonal bipyramids is forbidden. If the total number of nodal lattice sites is denoted as N, then the total number of trigonal bipyramidal units is exactly double, $N_u = 2N$, once periodic boundary conditions are imposed both in horizontal as well as vertical directions in the thermodynamic limit $N \to \infty$. The total Hamiltonian of the considered spin-electron model can be accordingly expressed as a sum of cell Hamiltonians $\hat{\mathcal{H}}_j$:

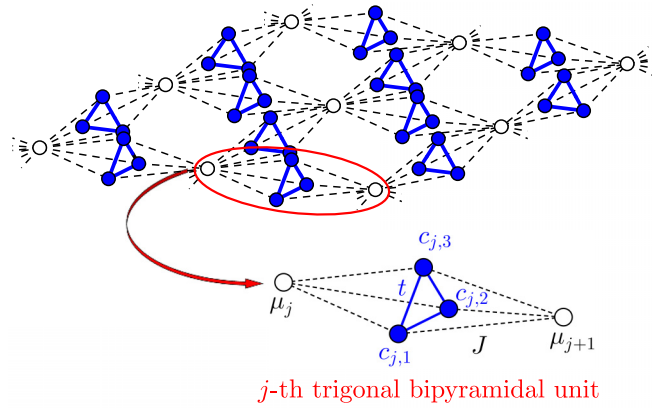

FIG. 1. A schematic representation of the coupled spin-electron model on a decorated square lattice composed of interconnected trigonal bipyramids. Empty (white) circles show nodal lattice sites occupied by the localized Ising spins $\mu = 1/2$, while filled (blue) circles denote decorating lattice sites available for mobile electrons. Solid (blue) lines illustrate hopping paths t of the mobile electrons, while dashed (black) lines show the Ising-type interaction J between the nodal Ising spins and the mobile electrons from their nearest decorating sites.

$$\hat{\mathcal{H}} = \sum_{j=1}^{N_u} \hat{\mathcal{H}}_j, \tag{1}$$

whereas the cell Hamiltonian $\hat{\mathcal{H}}_j$ contains all interaction terms inherent to the jth trigonal bipyramid:

$$\begin{aligned}\hat{\mathcal{H}}_j = &-t \sum_{\sigma\in\{\uparrow,\downarrow\}} \sum_{k=1}^{3} (\hat{c}^{\dagger}_{j,k,\sigma} \hat{c}_{j,k+1,\sigma} + \mathrm{H.c.}) \\ &-\frac{J}{2} \sum_{k=1}^{3} (\hat{n}_{j,k,\uparrow} - \hat{n}_{j,k,\downarrow})\big(\hat{\mu}^z_j + \hat{\mu}^z_{j+1}\big) \\ &+U \sum_{k=1}^{3} \hat{n}_{j,k,\uparrow}\hat{n}_{j,k,\downarrow}. \end{aligned} \tag{2}$$

In above, $\hat{c}^{\dagger}_{j,k,\sigma}$ ($\hat{c}_{j,k,\sigma}$) represents fermionic creation (annihilation) operator for mobile electrons with the spin $\sigma \in \{\uparrow, \downarrow\}$ ($\uparrow$ labels the spin state $1/2$, while $\downarrow$ labels the spin state $-1/2$) at the kth site of the jth triangular bipyramid,

$\hat{n}_{j,k,\sigma} = \hat{c}^{\dagger}_{j,k,\sigma}\hat{c}_{j,k,\sigma}$ is the fermion number operator, and $\hat{\mu}^z_j$ is the z component of the spin-1/2 operator corresponding to the Ising spin placed at the jth nodal lattice site. The parameter $t > 0$ takes into account the kinetic energy of mobile electrons performing a quantum-mechanical hopping within an individual triangular plaquette, $J > 0$ ($J < 0$) stands for the ferromagnetic (antiferromagnetic) Ising-type interaction between the Ising spins and its nearest-neighbor electrons, and $U > 0$ is the on-site Coulomb repulsion between two electrons occupying the same lattice site of a decorated triangular plaquette. Finally, the periodic boundary conditions $\hat{c}^{\dagger}_{j,4,\sigma} \equiv \hat{c}^{\dagger}_{j,1,\sigma}$ ($\hat{c}_{j,4,\sigma} \equiv \hat{c}_{j,1,\sigma}$) and $\hat{\mu}^z_{N_u+1} \equiv \hat{\mu}^z_1$ are assumed for the sake of simplicity of further calculations.

A. Energy spectrum of the cell Hamiltonian

The specific form of the cell Hamiltonian $\hat{\mathcal{H}}_j$ clearly indicates its invariance against the translation of the nodal lattice sites $\hat{\mu}^z_j \to \hat{\mu}^z_{j'}$ ($j \neq j'$). Moreover, the operators $\hat{n}_{j,\sigma} = \sum_{k=1}^{3}\hat{n}_{j,k,\sigma}$ and $\hat{S}^z_j = \sum_{k=1}^{3}\hat{S}^z_{j,k} = \sum_{k=1}^{3}(\hat{n}_{j,k,\uparrow} - \hat{n}_{j,k,\downarrow})/2$ emergent in Eq. (2), which correspond to the total number of mobile electrons with the spin σ and z component of the total spin per triangular plaquette, represent conserved quantities with well-defined quantum numbers $n_{j,\sigma} = \{0, 1, 2\}$ and $S^z_j = \{-1, 0, 1\}$, respectively. These facts imply validity of the following commutation relations:

$$[\hat{\mathcal{H}}_j, \hat{\mathcal{H}}_{j'}] = 0, \quad [\hat{\mathcal{H}}_j, \hat{n}_{j,\sigma}] = 0, \quad [\hat{\mathcal{H}}_j, \hat{S}^z_j] = 0. \tag{3}$$

The first commutation relation indicates that it is sufficient to find a full energy spectrum of the cell Hamiltonian (2) in order to treat exactly the coupled spin-electron model, because the relevant eigenstates can be simply extended to the whole system. The exact calculation can be performed in the two-site Hilbert subspace corresponding to the triangular plaquette from the jth unit cell, which can be divided into three disjoint (orthogonal) subspaces with the fixed eigenvalues S^z_j of the z component of the total spin operator $\hat{S}^z_j$ due to the validity of the third commutation relation in Eq. (3):

$$\mathscr{H} = \mathscr{H}_{S^z_j=-1} \oplus \mathscr{H}_{S^z_j=0} \oplus \mathscr{H}_{S^z_j=1}, \tag{4}$$

where

$$\begin{aligned}
\mathscr{H}_{S^z_j=-1} &= \{c^{\dagger}_{j,1,\downarrow}c^{\dagger}_{j,2,\downarrow}|0\rangle, c^{\dagger}_{j,2,\downarrow}c^{\dagger}_{j,3,\downarrow}|0\rangle, c^{\dagger}_{j,3,\downarrow}c^{\dagger}_{j,1,\downarrow}|0\rangle\},\\
\mathscr{H}_{S^z_j=0} &= \{c^{\dagger}_{j,1,\uparrow}c^{\dagger}_{j,1,\downarrow}|0\rangle, c^{\dagger}_{j,2,\uparrow}c^{\dagger}_{j,2,\downarrow}|0\rangle, c^{\dagger}_{j,3,\uparrow}c^{\dagger}_{j,3,\downarrow}|0\rangle,\\
&\quad c^{\dagger}_{j,1,\uparrow}c^{\dagger}_{j,2,\downarrow}|0\rangle, c^{\dagger}_{j,2,\uparrow}c^{\dagger}_{j,3,\downarrow}|0\rangle, c^{\dagger}_{j,3,\uparrow}c^{\dagger}_{j,1,\downarrow}|0\rangle,\\
&\quad c^{\dagger}_{j,1,\downarrow}c^{\dagger}_{j,2,\uparrow}|0\rangle, c^{\dagger}_{j,2,\downarrow}c^{\dagger}_{j,3,\uparrow}|0\rangle, c^{\dagger}_{j,3,\downarrow}c^{\dagger}_{j,1,\uparrow}|0\rangle\},\\
\mathscr{H}_{S^z_j=1} &= \{c^{\dagger}_{j,1,\uparrow}c^{\dagger}_{j,2,\uparrow}|0\rangle, c^{\dagger}_{j,2,\uparrow}c^{\dagger}_{j,3,\uparrow}|0\rangle, c^{\dagger}_{j,3,\uparrow}c^{\dagger}_{j,1,\uparrow}|0\rangle\}.
\end{aligned}$$

In the present notation, $|0\rangle$ labels the vacuum state. Consequently, searching for an energy spectrum of the unit Hamiltonian (2) can also be split into three independent calculations of the eigenvalues for two 3×3 and one 9×9 block matrices corresponding to the triangular plaquette with the z component of the total spin $S^z_j = \mp 1$ and $S^z_j = 0$, respectively. The diagonalization of the respective matrices results to the following unified analytical expression for the energy spectrum (the set of 10 different eigenvalues) of the unit Hamiltonian (2):

$$E_{l,j} = -JS^z_j(\mu^z_j + \mu^z_{j+1}) + \mathcal{E}_{l,j} \quad (l = 1, 2, \ldots, 10). \tag{5}$$

In above, $\mathcal{E}_{l,j}$ denotes the respective eigenvalue of the electron triangle in the jth bipyramidal unit (see the third column of Table I). The obtained energy spectrum (5) can be immediately employed for a comprehensive ground-state analysis as well as a rigorous evaluation of the partition function of the studied model.

B. Partition function

Taken into account the commutation relation between different unit Hamiltonians listed in Eq. (3), the partition function $\mathcal{Z}$ of the considered 2D spin-electron model can be partially factorized and expressed in terms of eigenenergies of the unit Hamiltonian (2):

$$\mathcal{Z} = \sum_{\{\mu_j\}}\prod_{j=1}^{N_u}\mathrm{Tr}_j\, e^{-\beta\hat{\mathcal{H}}_j} = \sum_{\{\mu_j\}}\prod_{j=1}^{N_u}\sum_{l=1}^{10} g_l\, e^{-\beta E_{l,j}}. \tag{6}$$

In above, $\beta = 1/(k_{\mathrm{B}}T)$, k_{B} is the Boltzmann's constant, T is the absolute temperature of the system, the symbol $\sum_{\{\mu_j\}}$ denotes the summation over all possible spin states of the nodal Ising spins, the product symbol $\prod_{j=1}^{N_u}$ runs over all bipyramidal units, and Tr_j stands for the trace over all possible degrees of freedom of two mobile electrons delocalized over the jth triangular cluster of the appropriate bipyramidal unit. Finally, the summation symbol $\sum_{l=1}^{10}$ counts all eigenenergies of the unit Hamiltonian (2) given by Eq. (5), whereas g_l denotes the degeneracy of a given energy level $E_{l,j}$. After performing the summation $\sum_{l=1}^{10}$, one obtains the effective Boltzmann's weight $w(\mu^z_j, \mu^z_{j+1})$, whose explicit form gives the opportunity to use the generalized decoration-iteration mapping transformation [16–19]:

$$\begin{aligned}
w(\mu^z_j, \mu^z_{j+1}) &= \sum_{l=1}^{10} g_l\, e^{-\beta E_{l,j}} = 2e^{\beta t} + e^{-2\beta t}\\
&\quad + 2(2e^{\beta t} + e^{-2\beta t})\cosh\left[\beta J\left(\mu^z_j + \mu^z_{j+1}\right)\right]\\
&\quad + 4e^{-\beta(t+U)/2}\cosh\left[\frac{\beta}{2}\sqrt{(U-t)^2 + 8t^2}\right]\\
&\quad + 2e^{\beta(2t-U)/2}\cosh\left[\frac{\beta}{2}\sqrt{(U+2t)^2 + 32t^2}\right]\\
&= Ae^{\beta J_{\mathrm{eff}}\mu^z_j\mu^z_{j+1}}.
\end{aligned} \tag{7}$$

An essence of the used algebraic mapping method lies in substituting all degrees of freedom of the mobile electrons by a novel effective Ising-type coupling J_{eff} between remaining nodal Ising spins. The mapping parameters A and J_{eff} emerging in the last line of Eq. (7) are determined by "self-consistency" of the used decoration-iteration transformation:

$$A = \sqrt{w_0 w_1}, \quad J_{\mathrm{eff}} = 2k_{\mathrm{B}}T\ln\left(\frac{w_1}{w_0}\right). \tag{8}$$

In above, $w_0 = w(\pm 1/2, \mp 1/2)$ and $w_1 = w(\pm 1/2, \pm 1/2)$.

After substituting Eq. (7) into Eq. (6) one may obtain the rigorous relation between the partition function $\mathcal{Z}$ of the

TABLE I. The set of 10 different energy eigenvalues $\mathcal{E}_{l,j}$ of a triangular plaquette from the jth bipyramidal unit corresponding to the cell Hamiltonian (2), the corresponding degeneracy g_l and the eigenvector $|\phi_l\rangle_j$ ($|\phi_l^{L,R}\rangle_j$). The superscripts L and R in the eigenvectors $|\phi_2^{L,R}\rangle_j$, $|\phi_4^{L,R}\rangle_j$, $|\phi_{10}^{L,R}\rangle_j$ label the left- and right-hand side chiral degrees of freedom of the electron pair at the jth triangular cluster, respectively. The mixing angles φ_{5-8} in the eigenvectors $|\phi_{5-8}\rangle_j$ are defined through the relations $\tan\varphi_l = \frac{\sqrt{2}}{4t}(U-\mathcal{E}_{l,j})$ for $l = 5, 6$ and $\tan\varphi_l = \frac{\sqrt{2}}{2t}(U-\mathcal{E}_{l,j})$ for $l = 7, 8$.

l	S_j^z	$\mathcal{E}_{l,j}$	g_l	Eigenvector
1	-1	$2t$	1	$\|\phi_1\rangle_j = \frac{1}{\sqrt{3}}(c^\dagger_{j,1,\downarrow}c^\dagger_{j,2,\downarrow} + c^\dagger_{j,2,\downarrow}c^\dagger_{j,3,\downarrow} + c^\dagger_{j,3,\downarrow}c^\dagger_{j,1,\downarrow})\|0\rangle$
2		$-t$	2	$\|\phi_2^{L,R}\rangle_j = \begin{cases} \frac{1}{\sqrt{3}}(c^\dagger_{j,1,\downarrow}c^\dagger_{j,2,\downarrow} + e^{2\pi\mathrm{i}/3}c^\dagger_{j,2,\downarrow}c^\dagger_{j,3,\downarrow} + e^{4\pi\mathrm{i}/3}c^\dagger_{j,3,\downarrow}c^\dagger_{j,1,\downarrow})\|0\rangle \\ \frac{1}{\sqrt{3}}(c^\dagger_{j,1,\downarrow}c^\dagger_{j,2,\downarrow} + e^{4\pi\mathrm{i}/3}c^\dagger_{j,2,\downarrow}c^\dagger_{j,3,\downarrow} + e^{2\pi\mathrm{i}/3}c^\dagger_{j,3,\downarrow}c^\dagger_{j,1,\downarrow})\|0\rangle \end{cases}$
3	0	$2t$	1	$\|\phi_3\rangle_j = \frac{1}{\sqrt{6}}(c^\dagger_{j,1,\uparrow}c^\dagger_{j,2,\downarrow} + c^\dagger_{j,2,\uparrow}c^\dagger_{j,3,\downarrow} + c^\dagger_{j,3,\uparrow}c^\dagger_{j,1,\downarrow} + c^\dagger_{j,1,\downarrow}c^\dagger_{j,2,\uparrow} + c^\dagger_{j,2,\downarrow}c^\dagger_{j,3,\uparrow} + c^\dagger_{j,3,\downarrow}c^\dagger_{j,1,\uparrow})\|0\rangle$
4		$-t$	2	$\|\phi_4^{L,R}\rangle_j = \begin{cases} \frac{1}{\sqrt{6}}\big[c^\dagger_{j,1,\uparrow}c^\dagger_{j,2,\downarrow} + c^\dagger_{j,1,\downarrow}c^\dagger_{j,2,\uparrow} + e^{2\pi\mathrm{i}/3}(c^\dagger_{j,2,\uparrow}c^\dagger_{j,3,\downarrow} + c^\dagger_{j,2,\downarrow}c^\dagger_{j,3,\uparrow}) \\ \quad + e^{4\pi\mathrm{i}/3}(c^\dagger_{j,3,\uparrow}c^\dagger_{j,1,\downarrow} + c^\dagger_{j,3,\downarrow}c^\dagger_{j,1,\uparrow})\big]\|0\rangle \\ \frac{1}{\sqrt{6}}\big[c^\dagger_{j,1,\uparrow}c^\dagger_{j,2,\downarrow} + c^\dagger_{j,1,\downarrow}c^\dagger_{j,2,\uparrow} + e^{4\pi\mathrm{i}/3}(c^\dagger_{j,2,\uparrow}c^\dagger_{j,3,\downarrow} + c^\dagger_{j,2,\downarrow}c^\dagger_{j,3,\uparrow}) \\ \quad + e^{2\pi\mathrm{i}/3}(c^\dagger_{j,3,\uparrow}c^\dagger_{j,1,\downarrow} + c^\dagger_{j,3,\downarrow}c^\dagger_{j,1,\uparrow})\big]\|0\rangle \end{cases}$
5		$\frac{U}{2} - t + \frac{1}{2}\sqrt{(U+2t)^2+32t^2}$	1	$\|\phi_5\rangle_j = \frac{1}{\sqrt{6}}\big[\sin\varphi_5 \sum_{k=1}^{3}(c^\dagger_{j,k,\uparrow}c^\dagger_{j,k+1,\downarrow} - c^\dagger_{j,k,\downarrow}c^\dagger_{j,k+1,\uparrow}) + \sqrt{2}\cos\varphi_5 \sum_{k=1}^{3} c^\dagger_{j,k,\uparrow}c^\dagger_{j,k,\downarrow}\big]\|0\rangle$
6		$\frac{U}{2} - t - \frac{1}{2}\sqrt{(U+2t)^2+32t^2}$	1	$\|\phi_6\rangle_j = \frac{1}{\sqrt{6}}\big[\sin\varphi_6 \sum_{k=1}^{3}(c^\dagger_{j,k,\uparrow}c^\dagger_{j,k+1,\downarrow} - c^\dagger_{j,k,\downarrow}c^\dagger_{j,k+1,\uparrow}) + \sqrt{2}\cos\varphi_6 \sum_{k=1}^{3} c^\dagger_{j,k,\uparrow}c^\dagger_{j,k,\downarrow}\big]\|0\rangle$
7		$\frac{U}{2} + \frac{t}{2} + \frac{1}{2}\sqrt{(U-t)^2+8t^2}$	2	$\|\phi_7\rangle_j = \begin{cases} \frac{1}{2}\big[\sin\varphi_7(c^\dagger_{j,1,\downarrow}c^\dagger_{j,2,\uparrow} - c^\dagger_{j,1,\uparrow}c^\dagger_{j,2,\downarrow} - c^\dagger_{j,3,\downarrow}c^\dagger_{j,1,\uparrow} + c^\dagger_{j,3,\uparrow}c^\dagger_{j,1,\downarrow}) \\ \quad +\sqrt{2}\cos\varphi_7(c^\dagger_{j,3,\uparrow}c^\dagger_{j,3,\uparrow} - c^\dagger_{j,2,\uparrow}c^\dagger_{j,2,\downarrow})\big]\|0\rangle \\ \frac{1}{\sqrt{12}}\big\{\sin\varphi_7\big[\sum_{k=1}^{2}(c^\dagger_{j,2k-1,\uparrow}c^\dagger_{j,2k,\downarrow} - c^\dagger_{j,2k-1,\downarrow}c^\dagger_{j,2k,\uparrow}) - 2(c^\dagger_{j,2,\uparrow}c^\dagger_{j,3,\downarrow} - c^\dagger_{j,2,\downarrow}c^\dagger_{j,3,\uparrow})\big] \\ \quad +\sqrt{2}\cos\varphi_7(2c^\dagger_{j,1,\uparrow}c^\dagger_{j,1,\uparrow} - c^\dagger_{j,2,\uparrow}c^\dagger_{j,2,\uparrow} - c^\dagger_{j,3,\uparrow}c^\dagger_{j,3,\downarrow})\big\}\|0\rangle \end{cases}$
8		$\frac{U}{2} + \frac{t}{2} - \frac{1}{2}\sqrt{(U-t)^2+8t^2}$	2	$\|\phi_8\rangle_j = \begin{cases} \frac{1}{2}\big[\sin\varphi_8(c^\dagger_{j,1,\downarrow}c^\dagger_{j,2,\uparrow} - c^\dagger_{j,1,\uparrow}c^\dagger_{j,2,\downarrow} - c^\dagger_{j,3,\downarrow}c^\dagger_{j,1,\uparrow} + c^\dagger_{j,3,\uparrow}c^\dagger_{j,1,\downarrow}) \\ \quad +\sqrt{2}\cos\varphi_8(c^\dagger_{j,3,\uparrow}c^\dagger_{j,3,\uparrow} - c^\dagger_{j,2,\uparrow}c^\dagger_{j,2,\downarrow})\big]\|0\rangle \\ \frac{1}{\sqrt{12}}\big\{\sin\varphi_8\big[\sum_{k=1}^{2}(c^\dagger_{j,2k-1,\uparrow}c^\dagger_{j,2k,\downarrow} - c^\dagger_{j,2k-1,\downarrow}c^\dagger_{j,2k,\uparrow}) - 2(c^\dagger_{j,2,\uparrow}c^\dagger_{j,3,\downarrow} - c^\dagger_{j,2,\downarrow}c^\dagger_{j,3,\uparrow})\big] \\ \quad +\sqrt{2}\cos\varphi_8(2c^\dagger_{j,1,\uparrow}c^\dagger_{j,1,\uparrow} - c^\dagger_{j,2,\uparrow}c^\dagger_{j,2,\uparrow} - c^\dagger_{j,3,\uparrow}c^\dagger_{j,3,\downarrow})\big\}\|0\rangle \end{cases}$
9	1	$2t$	1	$\|\phi_9\rangle_j = \frac{1}{\sqrt{3}}(c^\dagger_{j,1,\uparrow}c^\dagger_{j,2,\uparrow} + c^\dagger_{j,2,\uparrow}c^\dagger_{j,3,\uparrow} + c^\dagger_{j,3,\uparrow}c^\dagger_{j,1,\uparrow})\|0\rangle$
10		$-t$	2	$\|\phi_{10}^{L,R}\rangle_j = \begin{cases} \frac{1}{\sqrt{3}}(c^\dagger_{j,1,\uparrow}c^\dagger_{j,2,\uparrow} + e^{2\pi\mathrm{i}/3}c^\dagger_{j,2,\uparrow}c^\dagger_{j,3,\uparrow} + e^{4\pi\mathrm{i}/3}c^\dagger_{j,3,\uparrow}c^\dagger_{j,1,\uparrow})\|0\rangle \\ \frac{1}{\sqrt{3}}(c^\dagger_{j,1,\uparrow}c^\dagger_{j,2,\uparrow} + e^{4\pi\mathrm{i}/3}c^\dagger_{j,2,\uparrow}c^\dagger_{j,3,\uparrow} + e^{2\pi\mathrm{i}/3}c^\dagger_{j,3,\uparrow}c^\dagger_{j,1,\uparrow})\|0\rangle \end{cases}$

coupled spin-electron model given by the Hamiltonian (2) and the partition function $\mathcal{Z}_{\mathrm{IM}}$ of the corresponding spin-1/2 Ising square lattice given by the Hamiltonian $\mathcal{H}_{\mathrm{IM}} = -J_{\mathrm{eff}}\sum_{\langle j,n\rangle}^{N_u}\mu_j^z\mu_n^z$:

$$\mathcal{Z}(T,t,J,U) = A^{N_u}\mathcal{Z}_{\mathrm{IM}}(T,J_{\mathrm{eff}}). \tag{9}$$

The mapping relation (9) formally closes the rigorous solution of the considered spin-electron model, because the partition function $\mathcal{Z}_{\mathrm{IM}}$ of the spin-1/2 Ising model on a square lattice was exactly calculated in the seminal paper by Onsager [62–64].

C. Basic thermodynamic quantities and critical temperature

The mapping relation (9) gives an opportunity to rigorously calculate all basic thermodynamic quantities, as well as a critical temperature of the considered spin-electron model. To be specific, the numerical results for the Helmholtz free energy F, and subsequently for the entropy S and the specific heat C can be obtained by means of the following fundamental thermodynamic relations:

$$F = -k_{\mathrm{B}}T\ln\mathcal{Z}, \quad S = -\frac{\partial\mathcal{F}}{\partial T}, \quad C = -T\frac{\partial^2\mathcal{F}}{\partial T^2}. \tag{10}$$

Furthermore, by combining Eq. (9) with well-known exact theorems developed by Barry *et al.* [65–68] and the generalized Callen-Suzuki identity [69–71], the spontaneous sublattice magnetization per single localized Ising spin (m_{I}) and triangular plaquette (m_{e}) can also be acquired:

$$m_{\mathrm{I}} \equiv \langle\hat{\mu}_j^z\rangle = \langle\mu_j^z\rangle_{J_{\mathrm{eff}}} = m_{\mathrm{IM}}, \tag{11}$$

$$m_{\mathrm{e}} \equiv \langle\hat{S}_j^z\rangle = \frac{4}{w_1}(2e^{\beta t} + e^{-2\beta t})\sinh(\beta J)m_{\mathrm{IM}}. \tag{12}$$

In above, $\langle\ldots\rangle$ and $\langle\ldots\rangle_{J_{\mathrm{eff}}}$ denote the canonical ensemble averages performed within the investigated spin-electron model and the effective spin-1/2 Ising square lattice with the temperature-dependent nearest-neighbor coupling J_{eff} given by Eq. (8). The magnetization m_{IM} in Eqs. (11) and (12) represents the spontaneous single-site magnetization of the effective spin-1/2 Ising model on a square lattice, which can be exactly calculated from the well-known Yang's formula obtained in the 1950s [72]. Moreover, it is apparent from Eq. (12) that the sublattice magnetization m_{e} ascribed to the electron pair of a given bipyramidal unit is odd function of the exchange constant J. This implies that changing the ferromagnetic coupling ($J > 0$) between mobile electrons and localized spins to the antiferromagnetic one ($J < 0$) may merely cause

just a trivial spin flipping of the spin and electron sublattices with respect to each other, which is reflected in the change of signs of the corresponding magnetization $m_{\rm I}$ and $m_{\rm e}$ from identical to opposite ones, respectively. In view of the above notation, the total spontaneous magnetization m of the spin-electron model on a decorated square lattice composed of interconnected trigonal bipyramids normalized per unit cell can be defined as follows:

$$m = \frac{m_{\rm I} + 2m_{\rm e}}{2}. \tag{13}$$

Last, the rigorous criterion determining critical temperature of the considered spin-electron model also follows directly from the mapping relation (7). Namely, the formula (7) clearly indicates that the coupled spin-electron system may exhibit critical behavior only if the effective spin-1/2 Ising model on a square lattice with the temperature-dependent nearest-neighbor coupling $J_{\rm eff}$ is at a critical point. Thus, the critical temperature of the model defined through the Hamiltonian (1) can be straightforwardly obtained by setting the effective coupling $J_{\rm eff}$ listed in Eq. (8) to its critical value [62]:

$$\beta_c |J_{\rm eff}| = 2\ln(1+\sqrt{2}). \tag{14}$$

In above, $\beta_c = 1/(k_{\rm B}T_c)$, wherein T_c represents the critical temperature of the system.

D. Fermionic concurrence

Another quantity, which might be of particular interest for the investigated spin-electron model, is the fermionic concurrence. As will be demonstrated hereafter the fermionic concurrence provides a useful tool for a rigorous investigation of a degree of quantum correlations (bipartite entanglement) between two mobile electrons from the same triangular plaquette. The fermionic concurrence between two mobile electrons from the same unit cell can be examined from two perspectives – in the context of the charge or spin degrees of freedom of two quantum-mechanically entangled mobile electrons.

In general, the concurrence of any two-qubit system can be explicitly expressed by Wootters' formula [53,54]:

$$\mathcal{C} = \max\{0, \lambda_1 - \lambda_2 - \lambda_3 - \lambda_4\}, \tag{15}$$

where λ_i's ($i = 1{-}4$) are the eigenvalues of the Hermitian matrix $R_{j,l} = \sqrt{\sqrt{\rho_{j,l}}\tilde{\rho}_{j,l}\sqrt{\rho_{j,l}}}$ with $\tilde{\rho}_{j,l} = (\sigma^y \otimes \sigma^y)\rho^*_{j,l}(\sigma^y \otimes \sigma^y)$ sorted in descending order $\lambda_1 \geqslant \lambda_2 \geqslant \lambda_3 \geqslant \lambda_4$. Here $\rho_{j,l}$ labels the reduced density matrix of a qubit pair occupying the jth and lth lattice sites, which can be obtained from the full density matrix ρ by tracing out degrees of freedom of all other sites except the jth and lth ones, $\rho^*_{j,l}$ is the complex conjugate of $\rho_{j,l}$, and σ^y is the usual Pauli matrix.

The total Hilbert space of a single electron pair is six-dimensional, while the Wootters' concept of the concurrence is applicable just to four-dimensional Hilbert spaces. However, one may first separate charge and spin degrees of freedom of the electron pairs in order to calculate a degree of the bipartite entanglement within the respective four-dimensional Hilbert subspaces [55,56]. As a matter of fact, the charge concurrence measuring a degree of the bipartite entanglement between charge degrees of freedom of two mobile electrons can be rigorously evaluated in the eponymous two-site Hilbert subspace $\{|0,0\rangle, |0,\uparrow\rangle, |\uparrow,0\rangle, |\uparrow,\uparrow\rangle\}$ (or, equivalently, $\{|0,0\rangle, |0,\downarrow\rangle, |\downarrow,0\rangle, |\downarrow,\downarrow\rangle\}$). On the other hand, one may further distinguish two types of spin concurrences related to spin degrees of freedom of the mobile electrons. The single-spin concurrence determines a degree of the bipartite entanglement within the particular subspace spanned over four basis states with nonzero local magnetization $\{|\uparrow,\uparrow\rangle, |\uparrow,\downarrow\rangle, |\downarrow,\uparrow\rangle, |\downarrow,\downarrow\rangle\}$. Contrary to this, the zero-spin concurrence measures a degree of quantum correlations within the particular subspace spanned over four nonmagnetic (ionic) basis states $\{|0,0\rangle, |0,\uparrow\downarrow\rangle, |\uparrow\downarrow,0\rangle, |\uparrow\downarrow,\uparrow\downarrow\rangle\}$. In any of above three subspaces, the reduced density matrix associated with an electron pair delocalized over, e.g., kth and $(k{+}1)$st sites of the jth decorating triangular plaquette, takes the identical α form:

$$\rho^{\alpha}_{k,k+1} = \begin{bmatrix} u^{\alpha}_1 & 0 & 0 & 0 \\ 0 & v^{\alpha}_1 & z^{\alpha} & 0 \\ 0 & (z^{\alpha})^* & v^{\alpha}_2 & 0 \\ 0 & 0 & 0 & u^{\alpha}_2 \end{bmatrix} \quad (\alpha = c, s, 0). \tag{16}$$

Here the superscripts c, s, 0 stand for the charge, single-spin, and zero-spin subspaces, respectively. The nonzero elements of the individual density matrices (16) ascribed to three respective subspaces are given by the following formulas in the charge subspace:

$$u^c_1 = \langle (1-\hat{n}_{j,k,\uparrow})(1-\hat{n}_{j,k+1,\uparrow})\rangle, \tag{17a}$$
$$u^c_2 = \langle \hat{n}_{j,k,\uparrow}\hat{n}_{j,k+1,\uparrow}\rangle, \tag{17b}$$
$$v^c_1 = \langle \hat{n}_{j,k,\uparrow}(1-\hat{n}_{j,k+1,\uparrow})\rangle, \tag{17c}$$
$$v^c_2 = \langle (1-\hat{n}_{j,k,\uparrow})\hat{n}_{j,k+1,\uparrow}\rangle, \tag{17d}$$
$$z^c = (z^c)^* = \langle \hat{c}^{\dagger}_{j,k,\uparrow}\hat{c}_{j,k+1,\uparrow}\rangle, \tag{17e}$$

the single-spin subspace:

$$u^s_1 = \langle \hat{n}_{j,k,\uparrow}(1-\hat{n}_{j,k,\downarrow})\hat{n}_{j,k+1,\uparrow}(1-\hat{n}_{j,k+1,\downarrow})\rangle, \tag{18a}$$
$$u^s_2 = \langle (1-\hat{n}_{j,k,\uparrow})\hat{n}_{j,k,\downarrow}(1-\hat{n}_{j,k+1,\uparrow})\hat{n}_{j,k+1,\downarrow}\rangle, \tag{18b}$$
$$v^s_1 = \langle \hat{n}_{j,k,\uparrow}(1-\hat{n}_{j,k,\downarrow})(1-\hat{n}_{j,k+1,\uparrow})\hat{n}_{j,k+1,\downarrow}\rangle, \tag{18c}$$
$$v^s_2 = \langle (1-\hat{n}_{j,k,\uparrow})\hat{n}_{j,k,\downarrow}\hat{n}_{j,k+1,\uparrow}(1-\hat{n}_{j,k+1,\downarrow})\rangle, \tag{18d}$$
$$z^s = (z^s)^* = \langle \hat{c}^{\dagger}_{j,k+1,\uparrow}\hat{c}_{j,k+1,\downarrow}\hat{c}^{\dagger}_{j,k,\downarrow}\hat{c}_{j,k,\uparrow}\rangle, \tag{18e}$$

and the zero-spin subspace:

$$u^0_1 = \langle (1-\hat{n}_{j,k,\uparrow})(1-\hat{n}_{j,k+1,\uparrow})(1-\hat{n}_{j,k,\downarrow})(1-\hat{n}_{j,k+1,\downarrow})\rangle, \tag{19a}$$
$$u^0_2 = \langle \hat{n}_{j,k,\uparrow}\hat{n}_{j,k,\downarrow}\hat{n}_{j,k+1,\uparrow}\hat{n}_{j,k+1,\downarrow}\rangle, \tag{19b}$$
$$v^0_1 = \langle (1-\hat{n}_{j,k,\uparrow})(1-\hat{n}_{j,k,\downarrow})\hat{n}_{j,k+1,\uparrow}\hat{n}_{j,k+1,\downarrow}\rangle, \tag{19c}$$
$$v^0_2 = \langle \hat{n}_{j,k,\uparrow}\hat{n}_{j,k,\downarrow}(1-\hat{n}_{j,k+1,\uparrow})(1-\hat{n}_{j,k+1,\downarrow})\rangle, \tag{19d}$$
$$z^0 = (z^0)^* = \langle \hat{c}^{\dagger}_{j,k,\uparrow}\hat{c}^{\dagger}_{j,k,\downarrow}\hat{c}_{j,k+1,\downarrow}\hat{c}_{j,k+1,\uparrow}\rangle, \tag{19e}$$

All statistical mean values entering into Eqs. (17a)–(19e) can be obtained in the same way as the spontaneous sublattice magnetization of the mobile electrons $m_{\rm e}$, i.e., by combining the generalized Callen-Suzuki identity [69–71] with the exact mapping relation (9). The partial fermionic concurrences quantifying the charge, single-spin and zero-spin bipartite

entanglement between the mobile electrons residing kth and $(k+1)$st site of the jth decorating triangular plaquette can alternatively be expressed as:

$$\mathcal{C}^{\alpha}_{k,k+1} = 2\max\{0, |z^{\alpha}| - \sqrt{u^{\alpha}_1 u^{\alpha}_2}\}. \tag{20}$$

It is also worthy to note that all statistical means values emergent in the sets of Eqs. (17a)–(17e), (18a)–(18e), (19a)–(19e) are, in fact, identical for all available pairs of lattice sites from a given decorating triangular plaquette. Owing to this fact, the same strength of the partial bipartite entanglement between the mobile electrons is detected for any pair of lattice sites belonging to the same decorating triangular plaquette, which means that one may contract specification of lattice sites from the definition of the partial concurrences $\mathcal{C}^{\alpha}_{1,2} = \mathcal{C}^{\alpha}_{2,3} = \mathcal{C}^{\alpha}_{3,1} = \mathcal{C}^{\alpha}$. Of course, the overall bipartite entanglement between two mobile electrons from the same triangular plaquette is given by a sum of its three contributions:

$$\mathcal{C} = \mathcal{C}^{c} + \mathcal{C}^{s} + \mathcal{C}^{0}, \tag{21}$$

which turns out to be a monotonic function of von Neumann entanglement entropy [56].

III. RESULTS AND DISCUSSION

In this section, we will proceed to a discussion of the most interesting numerical results for the proposed spin-electron model. Before doing so it is worthy to mention that all the relations derived in Sec. II are valid for ferromagnetic ($J > 0$) as well as antiferromagnetic ($J < 0$) Ising-type interaction, whereas the transformation $J \to -J$ merely causes a rather trivial change of relative orientation of the spins of the mobile electrons with respect to their nearest nodal Ising spins. Taking into account this fact one may set the absolute value of the Ising-type interaction $|J|$ as an energy unit when defining dimensionless quantities $t/|J|$, $U/|J|$, and $k_{\rm B}T/|J|$ measuring relative strengths of the hopping integral, Coulomb repulsion, and temperature, respectively.

A. Ground state

We start with the analysis of the ground state of the model, which can be determined directly from the energy spectrum (5) of the cell Hamiltonian (2) due to validity of the first commutation relation in Eq. (3). A systematic inspection of all available combinations of the Ising spins μ^z_j and μ^z_{j+1} reveals existence of two different macroscopically degenerate quantum ground states. The first one can be classified as the spontaneously long-range ordered ferro- or ferrimagnetic (FM) phase depending on whether the exchange coupling between the nodal Ising spins and mobile electrons is ferromagnetic $J > 0$ or antiferromagnetic $J < 0$, respectively. The FM ground state is unambiguously given by the following eigenvector and energy per unit cell:

$$|\mathrm{FM}\rangle = \prod_{j=1}^{N_u} \left\{ \begin{array}{l} \left|-\mathrm{sgn}(J)\frac{1}{2}\right\rangle_{\mu^z_j} \otimes \left|\phi^{L,R}_2\right\rangle_j \\ \left|\mathrm{sgn}(J)\frac{1}{2}\right\rangle_{\mu^z_j} \otimes \left|\phi^{L,R}_{10}\right\rangle_j \end{array} \right., \tag{22a}$$

$$E_{\rm FM} = -|J| - t. \tag{22b}$$

The second ground state can be classified as the disordered frustrated (FRU) phase given by the eigenvector and energy per unit cell:

$$|\mathrm{FRU}\rangle = \prod_{j=1}^{N_u} \left|\pm\frac{1}{2}\right\rangle_{\mu^z_j} \otimes |\phi_6\rangle_j, \tag{23a}$$

$$E_{\rm FRU} = \frac{U}{2} - t - \frac{1}{2}\sqrt{(U+2t)^2 + 32t^2}. \tag{23b}$$

In above, the product symbol $\prod_{j=1}^{N_u}$ runs over all bipyramidal units, the single-site ket vector $|\ldots\rangle_{\mu^z_j}$ determines a spin state of the localized Ising spin from the jth nodal lattice site, and the state vectors $|\phi^{L,R}_2\rangle_j$, $|\phi^{L,R}_{10}\rangle_j$, $|\phi_6\rangle_j$ are eigenstates of two mobile electrons from the jth decorating triangular plaquette quoted explicitly in Table I.

One can easily deduce from Eq. (22a) that the macroscopic degeneracy of the spontaneously ordered FM phase closely relates to two possible [left- (L) and right-hand side (R)] chiral degrees of freedom of two mobile electrons from triangular plaquettes, which may reside one of two energetically equivalent quantum ferromagnetic states $|\phi^{L,R}_2\rangle_j$ with the total spin $S^z_j = -1$ or $|\phi^{L,R}_{10}\rangle_j$ with $S^z_j = 1$. Depending on the actual spin arrangement of a couple of the mobile electrons, the localized Ising spins choose one out of two possible spin states $\mu^z_j = -1/2$ and $1/2$ in order to maintain the overall ferromagnetic (ferrimagnetic) spin arrangement for $J > 0$ ($J < 0$). These findings clearly indicate that the macroscopic degeneracy of the FM phase is proportional to the total number of the triangular plaquettes N_u, since it comes from their chiral degrees of freedom, namely 2^{N_u+1} due to a spin-flip (time-reversal) symmetry of the system. On the other hand, the overall macroscopic degeneracy of the disordered FRU phase is proportional to the total number of localized Ising spins 2^N, because its origin closely relates to a paramagnetic (frustrated) character of the nodal Ising spins being with equal probability in one of their two available spin states $\mu^z_j = -1/2$ and $1/2$ [see Eq. (23a)]. The paramagnetic character of the localized Ising spins results from a kinetically driven frustration caused by the antiferromagnetic spin alignment of the mobile electrons, which underlie a quantum superposition of six intrinsic antiferromagnetic and three nonmagnetic ionic states (see explicit expression of the corresponding state vector $|\phi_6\rangle_j$ in Table I).

As expected, the stability region of two ground states is strongly affected by a mutual interplay between the Ising-type coupling constant, Coulomb parameter and hopping term. The first two interaction parameters favor presence of the spontaneously ordered FM phase, while the hopping term stabilizes existence of the disordered FRU phase. As a matter of fact, the spontaneous long-range ordered FM phase is the respective ground state whenever a relative strength of the hopping amplitude $t/|J|$ is smaller that the boundary value:

$$\frac{t_b}{|J|} = \frac{1}{18}\sqrt{\left[\frac{U}{|J|} + 6\mathrm{sgn}(J)\right]^2 + 24\mathrm{sgn}(J)\frac{U}{|J|}} - \frac{1}{18}\frac{U}{|J|}. \tag{24}$$

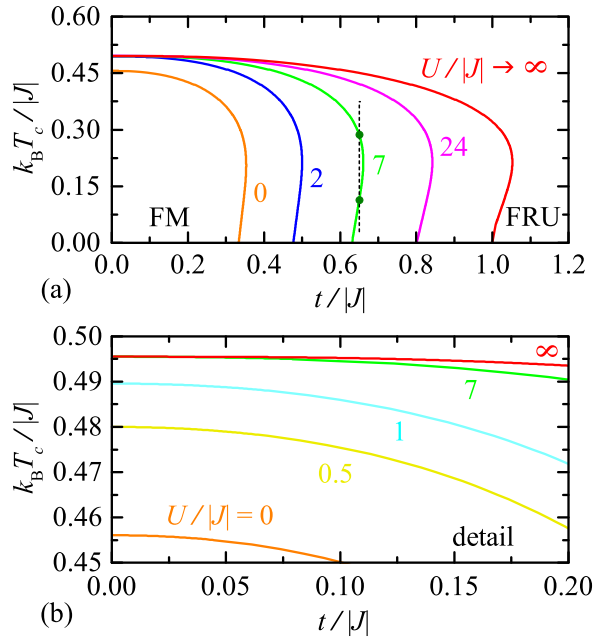

FIG. 2. The finite-temperature phase diagram showing the critical temperature $k_B T_c/|J|$ of the coupled spin-electron model on a decorated square lattice with interconnected triangular bipyramids as a function of the hopping parameter $t/|J|$ for several representative values of the Coulomb term $U/|J|$. A full phase diagram is depicted in panel (a) and its detail in a range of very low values of the hopping term $t/|J| \in (0, 0.2)$ in panel (b). The vertical short-dashed line in the panel (a) at $t/|J| = 0.65$ demonstrates double reentrant phase transitions at the critical temperatures $k_B T_{c1}/|J| \approx 0.113$ and $k_B T_{c2}/|J| \approx 0.286$ (dark green circles) for the particular value of the Coulomb term $U/|J| = 7$.

Otherwise the disordered FRU phase emerges in the ground state due to the kinetically driven frustration of the localized Ising spins.

B. Critical behavior

In this part, the critical temperature determining a breakdown of the spontaneous long-range order pertinent to the FM ground state will be explored in detail. All valuable information concerning with the critical behavior can be read from Fig. 2, where the critical temperature $k_B T_c/|J|$ associated with a continuous phase transition of the investigated spin-electron model is depicted as a function of the hopping parameter $t/|J|$ for a few fixed values of the Coulomb term $U/|J|$ in the parameter range covering both the FM and FRU ground states [Fig. 2(a)] and the limited range $t/|J| \in (0, 0.2)$ [Fig. 2(b)]. The plotted curves represent numerical solution of the exact critical condition (14). It is worth mentioning that the displayed critical temperature corresponds to the coupled spin-electron model with the ferromagnetic ($J > 0$) as well as antiferromagnetic ($J < 0$) Ising-type exchange constant, because the effective temperature-dependent interaction $J_{\rm eff}$ and hence also the critical temperature are even functions of J [see the second line of Eq. (7)].

As one can see from Fig. 2(a), the critical temperature delimiting a stability region of the spontaneous long-range FM order generally declines with increasing of the hopping term $t/|J|$ until it falls to zero value at the ground-state phase boundary (24) with the disordered FRU phase. The highest critical temperature can be accordingly acquired for any value of the Coulomb term in the limit of vanishingly small hopping term $t/|J| \to 0$. In this particular limit, the critical temperature shows a subtle rise from the asymptotic value found for the absent Coulomb repulsion $U/|J| = 0$:

$$\frac{k_B T_c}{|J|} = \left[\ln\left(\frac{2 + 5\sqrt{2} + \sqrt{50 + 20\sqrt{2}}}{2}\right)\right]^{-1} \approx 0.456, \tag{25}$$

up to the highest possible one acquired for the infinitely strong Coulomb repulsion $U/|J| \to \infty$:

$$\frac{k_B T_c}{|J|} = \left[\ln\left(1 + 2\sqrt{2} + 2\sqrt{2 + \sqrt{2}}\right)\right]^{-1} \approx 0.496. \tag{26}$$

It is noteworthy that the latter critical temperature (26) can be practically achieved already at finite but sufficiently strong on-site Coulomb repulsion $U/|J| \approx 7$ [see Fig. 2(b)].

Furthermore, for any value of the Coulomb term $U/|J|$ one can also find intriguing double reentrant phase transitions in a narrow range of the hopping parameter $t/|J| \gtrsim t_b/|J|$ being sufficiently close to the phase boundary between the FM and FRU phases [see Fig. 2(a), especially the case $U/|J| = 7$, for which the phenomenon is schematically demonstrated by the vertical short-dashed black line at $t/|J| = 0.65 \gtrsim (\sqrt{337} - 7)/18$, which intersects the corresponding second-order phase transition (solid green line) at two well-separated critical temperatures $k_B T_{c1}/|J| \approx 0.113$ and $k_B T_{c2}/|J| \approx 0.286$ (dark green circles)]. The observed double reentrant phase transitions clearly indicate that the spontaneous long-range FM spin arrangement can be thermally induced above the disordered FRU ground state through the "order by disorder" mechanism [73–75]. This type of reentrant phase transitions is entropically driven, because the spontaneously long-range FM phase has peculiarly higher macroscopic degeneracy due to chiral degrees of freedom of triangular plaquettes than the disordered FRU one, whose macroscopic degeneracy comes from spin degrees of freedom of the nodal Ising spins (we recall that the total number of triangular plaquettes is double compared to the number of the nodal Ising spins). Of course, the reentrance can be detected only in a close vicinity of the ground-state phase boundary, where the FRU and FM phases have very close internal energies. Another interesting finding is that the phenomenon is the more pronounced, the higher is the value of Coulomb parameter $U/|J|$. In the special case of infinitely strong Coulomb repulsion $U/|J| \to \infty$, at which the interplay between the hopping and Coulomb terms is equivalent to the effect of antiferromagnetic Heisenberg coupling [15], the region of double reentrant phase transitions is nearly doubled in comparison to the zero case $U/|J| = 0$.

C. Spontaneous magnetization

The reported ground-state spin arrangement and critical behavior of the investigated spin-electron model can be independently verified by temperature dependencies of the spontaneous magnetization.

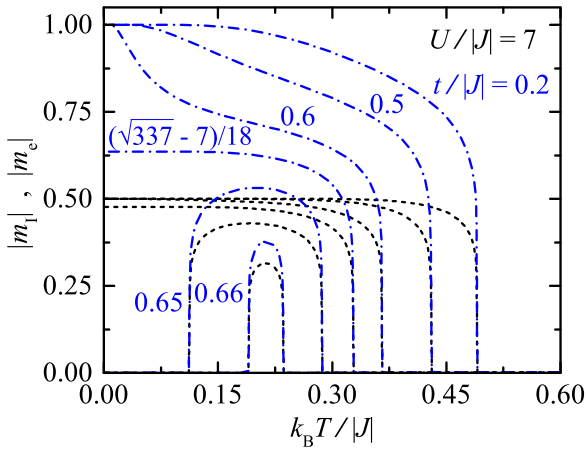

FIG. 3. Temperature variations of the spontaneous magnetization $|m_I|$ and $|m_e|$ of the spin and electron subsystems normalized per one localized Ising spin (short dashed black lines) and one pair of the mobile electrons (dash-dotted blue lines), respectively, for the fixed value of the Coulomb parameter $U/|J| = 7$ and several different values of the hopping term $t/|J|$.

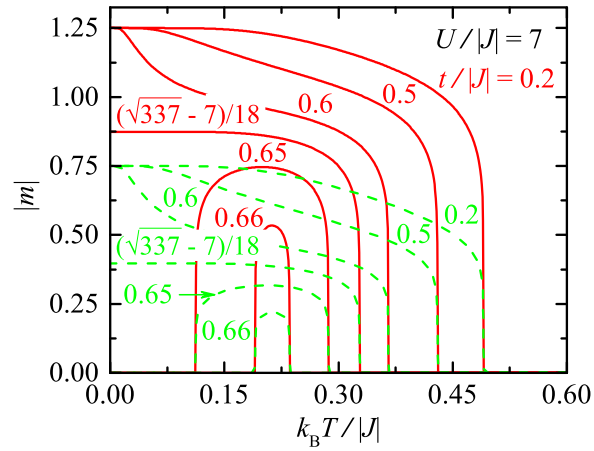

FIG. 4. Temperature variations of the total spontaneous magnetization $|m|$ per unit cell for the same values of the parameters $U/|J|$, $t/|J|$ as used in Fig. 3. Solid red (dashed green) lines display the total magnetization for the ferromagnetic (antiferromagnetic) interaction $J > 0$ ($J < 0$) between the localized Ising spins and mobile electrons.

We first focus our attention on temperature variations of spontaneous sublattice magnetization m_I and m_e normalized per one nodal Ising spin and electron pair, respectively. This study will bring insight into the effect of temperature fluctuations on ordering of spin and electron subsystems. Several typical temperature dependencies of both sublattice magnetization are shown in Fig. 3, where they are plotted in their absolute values $|m_I|$ (short dashed black lines) and $|m_e|$ (dash-dotted blue lines) to simultaneously reflect temperature-induced changes in the sublattice magnetization of the ferromagnetic ($J > 0$) as well as ferrimagnetic ($J < 0$) version of the model. In accordance with the ground-state analysis, the hopping amplitude $t/|J|$ smaller than the boundary value (24) prefers the spontaneous FM long-range order at zero temperature and both sublattice magnetization indeed start from their maximum zero-temperature asymptotic values $|m_I| = 0.5$ and $|m_e| = 1$. Both they gradually diminish on increasing of temperature and rapidly fall down to zero at a critical temperature according to the power law with the critical exponent $\beta_m = 1/8$ from the standard Ising universality class. However, there is an obvious difference in temperature variations of $|m_I|$ and $|m_e|$ at low and moderate temperatures. More specifically, the absolute value of the former magnetization $|m_I|$ remains almost constant over a relatively wide temperature range for any value $t/|J| < t_b/|J|$, while the latter $|m_e|$ falls down more steeply with increasing of temperature especially if the hopping term is close to $t/|J| \lesssim t_b/|J|$. This fact clearly implies that the electron subsystem is more sensitive with respect to temperature fluctuations than the spin subsystem.

It is noteworthy that both spontaneous sublattice magnetization start from the nontrivial zero-temperature asymptotic values $|m_I| \approx 0.477$ and $|m_e| \approx 0.636$ if the hopping term is fixed exactly at the ground-state boundary $t_b/|J|$ between the FM and FRU phases. The unsaturated values of the sublattice magnetization reflect a mutual coexistence of the FM and FRU phases, which consequently partially destroy a perfect spontaneous long-range order of both electron as well as spin subsystem. It is somewhat more surprising that spontaneous magnetization $|m_I|$ and $|m_e|$ of both subsystems display almost constant temperature dependencies in a relatively wide temperature range $k_BT/|J| < k_BT_c/|J|$, which indicates that the coexistence of the FM and FRU phases is thermally quite stable and it abruptly breaks down just slightly below the critical temperature [see the particular case $t_b/|J| = (\sqrt{337} - 7)/18 \approx 0.631$ in Fig. 3].

On the other hand, absence of the spontaneous magnetization is found at zero temperature for sufficiently strong hopping terms $t/|J| > t_b/|J|$, which prefer the disordered FRU ground state instead of the spontaneously ordered FM one. However, temperature dependencies of both sublattice magnetization $|m_I|$ and $|m_e|$ may display for not too strong hopping terms $t/|J| \gtrsim t_b/|J|$ an intriguing domelike temperature dependence pointing to emergence of the spontaneous long-range order at lower critical temperature and its breakdown at upper critical temperature (see the curves corresponding to $t/|J| = 0.65$ and 0.66 in Fig. 3). The observed nonmonotonous variations of $|m_I|$ and $|m_e|$ clearly corroborate an entropically driven activation of the spontaneous FM order above the disordered FRU ground state. Naturally, the afore-described temperature variations of the sublattice magnetization m_I and m_e significantly affect also temperature variations of the total spontaneous magnetization m normalized per bipyramidal unit cell, which can be considered as the relevant order parameter for the spontaneously long-range ordered FM phase regardless of the nature (sign) of the Ising-type coupling constant J. This statement is supported by Fig. 4, where temperature dependencies of the total magnetization m are depicted for the same values of the parameters $U/|J|$ and $t/|J|$ as used in Fig. 3 for the sublattice magnetization. In order to maintain the generality of the discussion, the absolute value of the total magnetization $|m|$ is plotted in Fig. 4 against temperature by considering the ferromagnetic exchange interaction $J > 0$ (solid red lines) and

the antiferromagnetic exchange constant $J < 0$ (dashed green lines) between the localized Ising spins and mobile electrons. Obviously, the plotted dependencies of the total magnetization $|m|$ faithfully follow predominantly temperature variations of the spontaneous magnetization of the electron subsystem $|m_e|$ including the remarkable nonmonotonous domelike dependence emergent for $t/|J| \gtrsim t_b/|J|$. The full saturation value $|m| = 1.25$ of the total magnetization is reached in the zero-temperature asymptotic limit for the hopping parameters $t/|J| < t_b/|J|$ just for the ferromagnetic coupling constant $J > 0$. This value reflects a perfect ferromagnetic spin alignment of the Ising and electron subsystems. On the other hand, the zero-temperature asymptotic value of the total magnetization starts from the unsaturated value $|m| = 0.75$, which agrees well with a perfect ferrimagnetic spin alignment of the spin and electron subsystems when the antiferromagnetic coupling constant $J < 0$ is assumed.

D. Specific heat and entropy

Next, we will turn our attention to temperature dependencies of the specific heat $C/(N_u k_B)$ and entropy $S/(N_u k_B)$ normalized per bipyramidal unit cell of the lattice, which are depicted in Fig. 5. In this figure, the values of the Coulomb term $U/|J|$ and the hopping parameter $t/|J|$ were selected so that the plotted curves are directly comparable to the finite-temperature phase diagram shown in Fig. 2 and temperature variations of the spontaneous magnetization plotted in Figs. 3 and 4.

Figure 5(a) illustrates temperature variations of the quantities $C/(N_u k_B)$ and $S/(N_u k_B)$ (in the inset) which are typical for the spontaneously ordered FM ground state and zero-temperature phase boundary between the FM and FRU ground states. In accordance to the finite-temperature phase diagram in Fig. 2, all plotted specific heat curves exhibit a single logarithmic divergence from the standard Ising universality class, which is associated with the continuous (second-order) phase transition between the spontaneously ordered FM and disordered paramagnetic (PM) phases. Apparently, the logarithmic divergence becomes the narrower, the closer the hopping parameter $t/|J|$ is selected to the ground-state boundary FM-FRU. Moreover, for $t/|J| \lesssim t_b/|J|$ the low-temperature part of the specific heat includes a notable round Schottky-type maximum [see the curve corresponding to $t/|J| = 0.6$ in Fig. 5(a)]. A comparison of the specific heat curves displayed in Fig. 5(a) with corresponding temperature dependencies of the entropy and sublattice magnetization shown in its inset and Fig. 3, respectively, clearly indicates that the observed Schottky peak originates from thermal excitations from the FM ground state to the low-lying excited state with the character of the disordered FRU phase. In accordance with this statement, the low-temperature Schottky-type maximum is gradually shifted toward zero temperature as the hopping term approaches the phase boundary between the FM and FRU phases conditioned by Eq. (24) and completely disappears when $t_b/|J|$ is reached [see the curve in Fig. 5(a) plotted for $t_b/|J| = (\sqrt{337} - 7)/18$].

More diverse temperature variations of the specific heat and entropy might be even expected when the hopping parameter $t/|J|$ drives the coupled spin-electron system to the disordered FRU ground state. Recall that this happens only if the hopping terms is greater than the boundary value $t_b/|J|$ given by Eq. (24). Several typical temperature variations of the specific heat $C/(N_u k_B)$ and entropy $S/(N_u k_B)$ corresponding to this parameter region are illustrated in Fig. 5(b). As one can see, the temperature variations of $C/(N_u k_B)$ may exhibit two pronounced round maxima and two logarithmic divergences if the value of the hopping term $t/|J| \gtrsim t_b/|J|$ is selected close enough to the ground-state phase boundary between the FM and FRU phases [see the curves corresponding to $t/|J| = 0.65$ and 0.66 in Fig. 5(b)]. A steep low-temperature variations of the entropy $S/(N_u k_B)$ shown in the inset of Fig. 5(b) convincingly evidence that the low-temperature round maximum can be viewed as the Schottky-type peak originating from vigorous thermal excitations from the FRU ground state to the FM excited state. On the contrary, high-temperature round maxima in specific heat curves come from extensive thermally induced excitations of very diverse character and it cannot be described by the Schottky theory. Two logarithmic divergences of the specific heat, which are present in between the round maxima, provide another independent confirmation of outstanding double

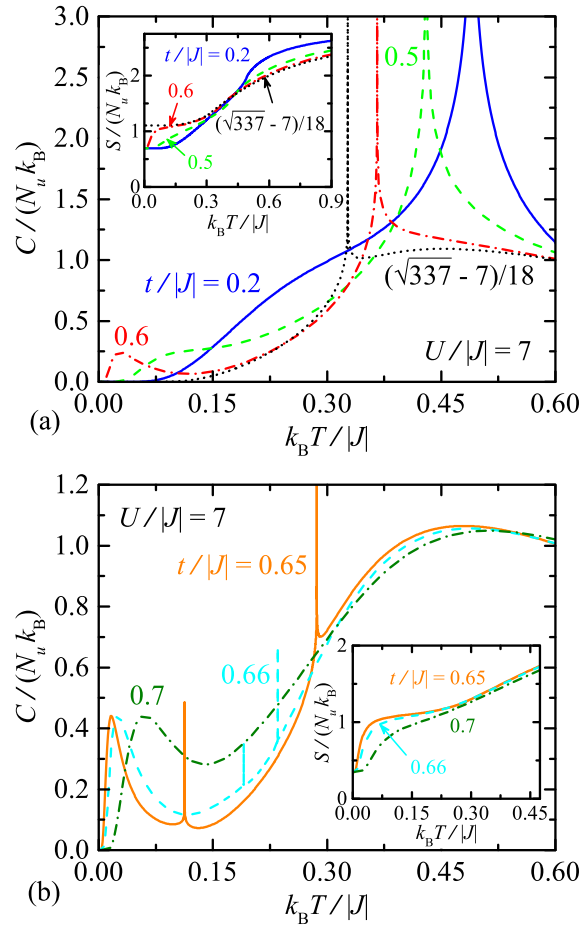

FIG. 5. Temperature dependencies of the specific heat and entropy (in the insets) per unit cell for the Coulomb term $U/|J| = 7$ and a few several different values of the hopping parameter $t/|J|$ typical for (a) the spontaneous FM ground state and the ground-state phase transition FM-FRU and (b) the disordered FRU ground state.

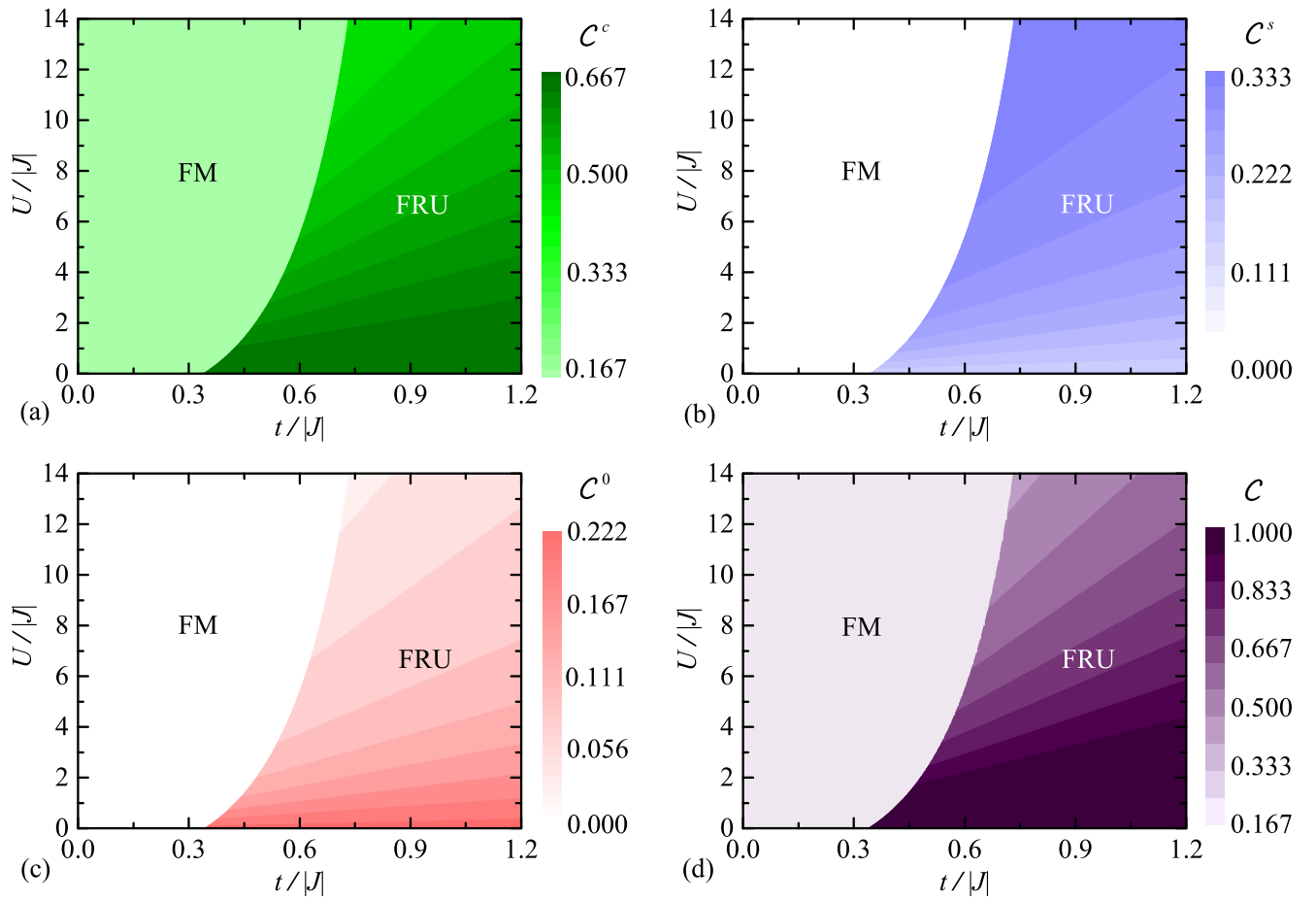

FIG. 6. Zero-temperature density plots of (a) the charge concurrence $\mathcal{C}^c$, (b) the single-spin concurrence $\mathcal{C}^s$, (c) the zero-spin concurrence $\mathcal{C}^0$, and (d) the overall concurrence $\mathcal{C}$ in the $t/|J| - U/|J|$ parameter plane of the investigated spin-electron model.

reentrant phase transitions emergent in a relatively narrow parameter region $t/|J| \gtrsim t_b/|J|$. These results perfectly coincide with the ones previously discussed at the finite-temperature phase diagram and temperature dependencies of the spontaneous sublattice and total magnetization [Figs. 2(a), 3, and 4]. In agreement with the previous findings, two marked logarithmic divergences of the specific heat gradually get closer to each other as the hopping term $t/|J|$ further increases until they completely coalesce at a certain value of the hopping term, above which only disordered FRU phase is realized. Consequently, the logarithmic divergence of the specific heat completely disappears from a thermal dependence of the specific heat due to a complete suppression of the spontaneous FM long-range order at zero as well as any nonzero temperature by the disordered FRU phase [see the curve corresponding to $t/|J| = 0.7$ in Fig. 5(b)].

E. Bipartite fermionic entanglement

In the last subsection we will investigate in detail a bipartite fermionic entanglement between two mobile electrons delocalized over the same triangular plaquette of the considered spin-electron model. To this end, we have used Eq. (20) to exactly calculate the charge ($\mathcal{C}^c$), single-spin ($\mathcal{C}^s$), and also zero-spin ($\mathcal{C}^0$) concurrences that quantify intensities of the bipartite entanglement between particles in eponymous subspaces. Zero-temperature asymptotic values of these three contributions to the overall concurrence $\mathcal{C}$ are explicitly given in Table II for both available FM and FRU ground states. Evidently, the bipartite entanglement between the mobile electrons comes within the FM ground state exclusively from the charge sector, while the single- and zero-spin sectors do not contribute to the entanglement at all. Contrary to this, the entanglement in the FRU ground state is distributed over all three sectors, whereas individual contributions basically depend on relative strengths of the interaction parameters $t/|J|$ and $U/|J|$ through the mixing angle φ_6 specified in Table I. For illustration, Fig. 6 displays in the $t/|J| - U/|J|$ parameter plane the zero-temperature density plots of all three partial concurrences $\mathcal{C}^c$, $\mathcal{C}^s$, $\mathcal{C}^0$, and the overall concurrence

TABLE II. Zero-temperature asymptotic values of the charge ($\mathcal{C}^c$), single-spin ($\mathcal{C}^s$), and zero-spin ($\mathcal{C}^0$) concurrences within two available ground states FM and FRU. The mixing angle φ_6 is explicitly given in Table I.

	$\mathcal{C}^c$	$\mathcal{C}^s$	$\mathcal{C}^0$
FM	$\frac{1}{6}$	0	0
FRU	$\frac{1}{3}\sin^2\varphi_6 + \frac{\sqrt{2}}{3}\sin 2\varphi_6$	$\frac{1}{3}\sin^2\varphi_6$	$\frac{2}{3}\cos^2\varphi_6$

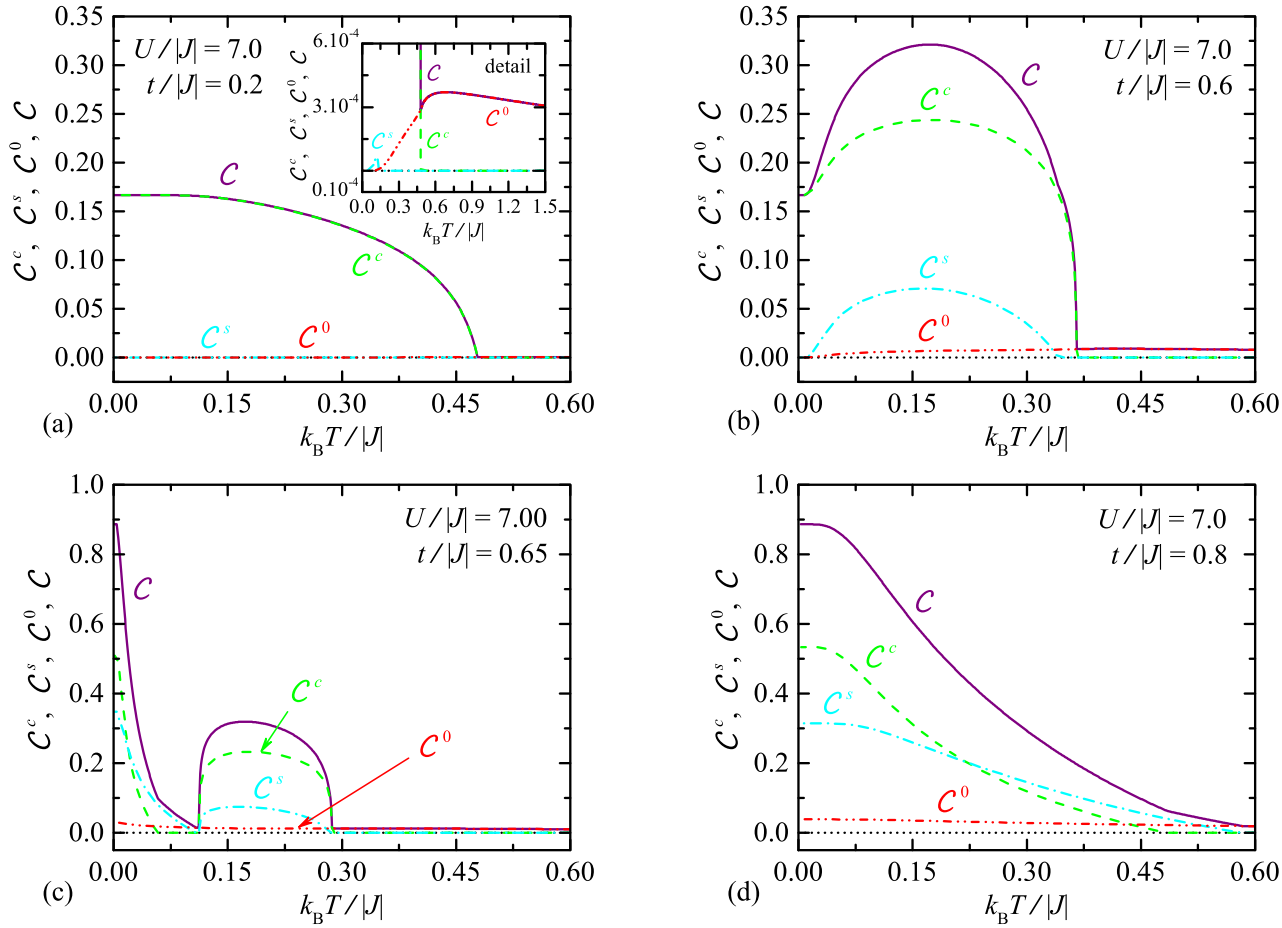

FIG. 7. Temperature dependencies of the charge concurrence $\mathcal{C}^c$, the single-spin concurrence $\mathcal{C}^s$, the zero-spin concurrence $\mathcal{C}^0$, and the overall concurrence $\mathcal{C}$ for the fixed Coulomb term $U/|J| = 7$ and four selected values of the hopping parameter $t/|J|$. Panels (a) and (b) show typical temperature variations of the concurrences that are typical for the spontaneous FM ground state, while panels (c) and (d) show the typical temperature variations of the quantities for the disordered FRU ground state.

$\mathcal{C}$ obtained by their summing. It can be easily understood from Fig. 6 that the strength of the overall bipartite entanglement between the mobile electrons from the same triangular plaquette as well as its three contributions from the charge, single-spin and zero-spin sectors are generally stronger in the FRU ground state than those in the FM ground state regardless of the values of the Coulomb term $U/|J|$ and/or the hopping parameter $t/|J|$. The entanglement present in the FM ground state is kept constant within whole stability region of the phase, while that in the FRU phase is generally promoted by the hopping term $t/|J|$, but weakened by the Coulomb repulsion $U/|J|$. The observed reduction of the bipartite entanglement is a direct consequence of a significant weakening of quantum correlations in the charge and zero-spin sectors invoked on strengthening of the Coulomb term $U/|J|$ though an opposite trend, albeit less intense, can be found in the single-spin sector [see Figs. 6(a)–6(c)].

To get an insight into the thermal resistance of the bipartite fermionic entanglement, some typical temperature variations of the overall concurrence and its three partial contributions are displayed in Fig. 7 for the fixed Coulomb term $U/|J| = 7$ and four different values of the hopping parameter $t/|J|$. Figures 7(a) and 7(b) capture the situation when the interplay between the interaction parameters $U/|J|$, $t/|J|$ enforces the spontaneously ordered FM ground state. It can be seen from these figures that the overall concurrence $\mathcal{C}$ is primarily governed at low and moderate temperatures by the charge contribution $\mathcal{C}^c$, which is gradually reduced on increasing of temperature at sufficiently low values of the hopping term $t/|J|$ [see Fig. 7(a)], or shows a striking initial temperature-induced rise due to thermal excitations from less entangled FM ground state to more entangled FRU excited state when the hopping amplitude $t/|J|$ is taken close enough to the phase boundary FM-FRU [see Fig. 7(b)]. It turns out, moreover, that the single-spin concurrence $\mathcal{C}^s$ also displays similar but slightly smaller temperature-induced rise, which becomes especially pronounced if the hopping term $t/|J|$ is selected sufficiently close to the ground-state phase boundary between the FM and FRU ground states emergent at $t_b/|J| \approx 0.631$. In any case, the charged concurrence $\mathcal{C}^c$ rapidly drops to zero at a certain temperature, above which the relevant temperature dependence of the overall concurrence is basically driven by a relatively small but nonzero zero-spin concurrence $\mathcal{C}^0$ [see the inset in Figs. 7(a) and 7(b)].

Figures 7(c) and 7(d) show typical temperature variations of the overall concurrence $\mathcal{C}$ and its three partial contributions

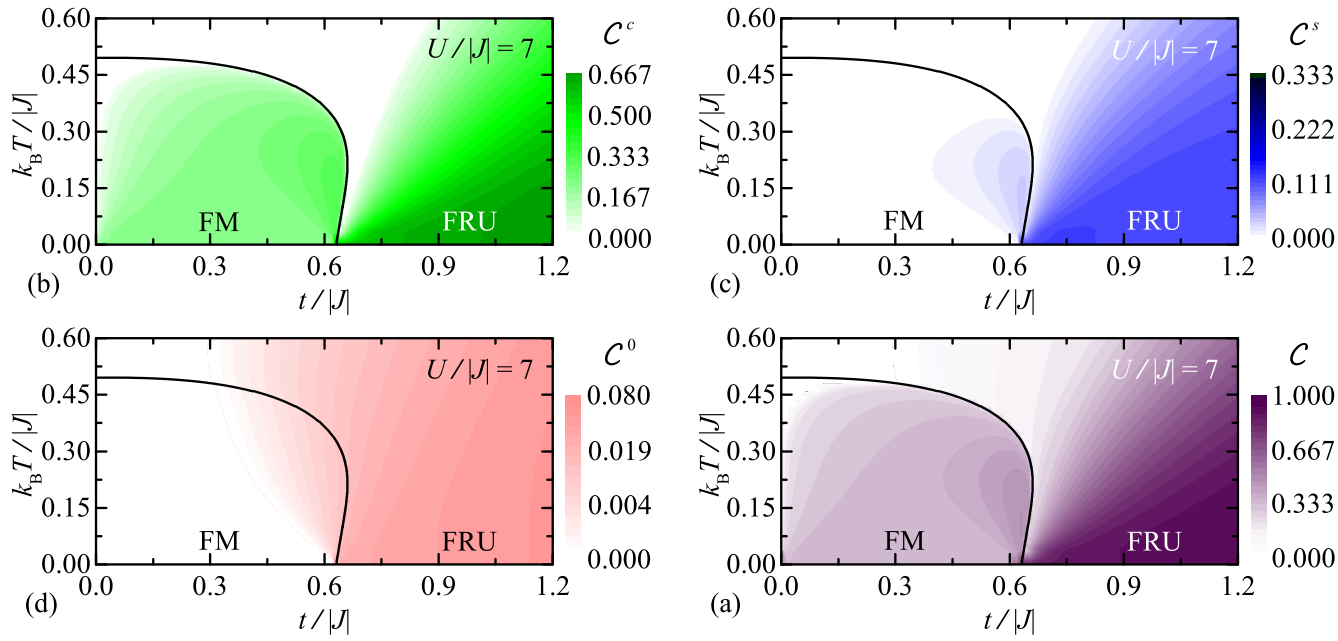

FIG. 8. Density plots of (a) the charge concurrence $\mathcal{C}^c$, (b) the single-spin concurrence $\mathcal{C}^s$, (c) the zero-spin concurrence $\mathcal{C}^0$, and (d) and the overall concurrence $\mathcal{C}$ in the $t/|J| - k_B T/|J|$ parameter plane for the fixed value of the Coulomb term $U/|J| = 7$. The black solid line represents the critical temperature $k_B T_c/|J|$, above which the spontaneous FM long-range order vanishes.

$\mathcal{C}^c$, $\mathcal{C}^s$, $\mathcal{C}^0$ for the hopping terms driving the investigated spin-electron model toward the FRU ground state. If the hopping term is selected slightly above the boundary value $t/|J| \gtrsim 0.631$, then the charge concurrence $\mathcal{C}^c$ displays a relatively steep decline down to zero in a low-temperature region, which is followed by a peculiar reentrant temperature dependence with a domelike shape observable in a range of moderate temperatures [see in Fig. 7(c)]. Evidently, the single-spin concurrence $\mathcal{C}^s$ exhibits qualitatively similar temperature dependence with exception of that it does not go to zero before the charge concurrence $\mathcal{C}^c$ enters the reentrant region. Note furthermore that the zero-spin concurrence $\mathcal{C}^0$ repeatedly provides the smallest contribution to the overall concurrence, which becomes relevant just at sufficiently high temperatures where the charged and single-spin contributions $\mathcal{C}^c$ and $\mathcal{C}^s$ completely diminish. It is quite obvious from Fig. 7(d) that the outstanding domelike temperature dependencies of the charge and single-spin concurrences disappear if one considers high-enough values of the hopping term $t/|J|$. Under this condition, the concurrences $\mathcal{C}^c$ and $\mathcal{C}^s$ generally exhibit a simple monotonous decline with increasing temperature, whereby the charge concurrence $\mathcal{C}^c$ decays more rapidly in comparison with the single-spin one $\mathcal{C}^s$. The zero-spin concurrence $\mathcal{C}^0$ still provides the smallest but nonzero contribution to the overall concurrence $\mathcal{C}$, which has features of the charge and single-spin concurrences with exception of the high-temperature region where it is driven by $\mathcal{C}^0$ [see Fig. 7(d)].

Last, we have depicted in Fig. 8 density plots of the charge, single-spin, zero-spin and total concurrences in the $t/|J| - k_B T/|J|$ plane for the fixed value of the Coulomb term $U/|J| = 7$ serving for global illustration. It can be seen from Figs. 8(a)–8(c) that the bipartite fermionic entanglement ascribed to the spontaneously ordered FM phase comes almost exclusively from the charge concurrence $\mathcal{C}^c$, because the single-spin concurrence $\mathcal{C}^s$ and the zero-spin one $\mathcal{C}^0$ only provide small negligible contributions in a vicinity of the phase boundary between the FM and FRU phases. It is also worthwhile to remark that nonzero values of the charge concurrence $\mathcal{C}^c$ are strictly delimited by the critical temperature $k_B T_c/|J|$ of the investigated coupled spin-electron system (black solid line), which determines a breakdown of the spontaneous FM long-range order. In opposite to this, all three contributions $\mathcal{C}^c$, $\mathcal{C}^s$, and $\mathcal{C}^0$ spread over much wider temperature range above the disordered FRU ground state.

IV. CONCLUSIONS

The present work deals with a coupled spin-electron model on a decorated square lattice composed of interconnected trigonal bipyramids, which is exactly solved by the generalized decoration-iteration transformation establishing a rigorous mapping correspondence with the effective spin-1/2 Ising model on a square lattice. In particular, we have comprehensively studied ground-state and finite-temperature phase diagrams, which are additionally complemented by a detailed analysis of the spontaneous magnetization and basic thermodynamic quantities (entropy, specific heat). Beside to this, the fermionic concurrence serving as a measure of bipartite entanglement between two mobile electrons has been exactly calculated. While the total fermionic concurrence is proportional to the entanglement entropy, its partial contributions referred to as the charge, single-spin and zero-spin concurrences shed light on the origin of the fermionic bipartite entanglement.

It has been demonstrated that the investigated spin-electron model exhibits two macroscopically degenerate quantum

ground states: the ferro- or ferrimagnetic phase (FM) and the frustrated one (FRU). The macroscopic degeneracy of the former ground state can be attributed to chiral degrees of freedom of the mobile electrons hopping within triangular plaquettes, while that of the latter ground state originates from the paramagnetic character of the localized Ising spins caused by a kinetically driven spin frustration. It surprisingly turned out that the FM phase with higher macroscopic degeneracy is spontaneously long-range ordered, while the FRU one is disordered in its character. The higher residual entropy of the macroscopically degenerate FRU phase is at origin of double reentrant phase transitions, which can be found in a relatively narrow parameter region sufficiently close but slightly above the ground-state phase boundary with the FRU ground state. The outstanding reentrant phase transitions have been independently verified by the respective temperature dependencies of the spontaneous magnetization and specific heat.

The most interesting finding of the present paper concerns with a detailed investigation of the bipartite fermionic entanglement quantified by the concept of the fermionic concurrence and its partial contributions. It has been verified that the bipartite fermionic entanglement within the spontaneously ordered FM phase predominantly comes from the charge sector and it persists up to the critical temperature, at which the spontaneous magnetization as the relevant order parameter vanishes. On the other hand, the charge, single-spin and zero-spin concurrences provide comparable contributions to the overall concurrence and hence, the bipartite fermionic entanglement spreads over much wider temperature range whenever the coupled spin-electron model is driven to the disordered FRU phase. It could be thus concluded that the disordered FRU state fits demanding requirements related to a stabilization of quantum entanglement and coherence as indispensable ground for a quantum computation much better than the spontaneously ordered FM phase. On the other hand, the chiral degrees of freedom of two electrons delocalized over triangular plaquettes within the ordered FM state could be potentially used for encoding qubits. Last, the striking reentrant phenomenon of the fermionic concurrence can be attributed to a higher macroscopic degeneracy of the spontaneously ordered FM ground state in comparison with the disordered FRU one.

ACKNOWLEDGMENTS

The work was financially supported by the Slovak Research and Development Agency under the Contract No. APVV-16-0186 and by the Ministry of Education, Science, Research and Sport of the Slovak Republic under Grant No. VEGA 1/0105/20.

[1] L. Jaeger, *The Second Quantum Revolution* (Springer Nature, Baar, Switzerland, 2018).
[2] L. K. Grover, Phys. Rev. Lett. **79**, 4709 (1997).
[3] P. W. Shor, SIAM J. Comput. **26**, 1484 (1997).
[4] P. Kok, W. J. Munro, K. Nemoto, T. C. Ralph, J. P. Dowling, and G. J. Milburn, Rev. Mod. Phys. **79**, 135 (2007).
[5] C. Monroe and J. Kim, Science **339**, 1164 (2013).
[6] G. Wendin, Rep. Prog. Phys. **80**, 106001 (2017).
[7] I. Oliveira, R. Sarthour, T. Bonagamba, E. Azevedo, and J. C. C. Freitas, *NMR Quantum Information Processing* (Elsevier, Amsterdam, 2007), pp. 137-181.
[8] V. Lahtinen and J. Pachos, SciPost Phys. **3**, 21 (2017).
[9] X. Mi, M. Benito, S. Putz, D. M. Zajac, J. M. Taylor, G. Burkard, and J. R. Petta, Nature (London) **555**, 599 (2018).
[10] D. P. DiVincenzo, *Scalable Quantum Computers* (Wiley-VCH, Weinheim, 2005).
[11] M. A. Nielsen and I. L. Chuang, *Quantum Computation and Quantum Information* (Cambridge University Press, Cambridge, 2010).
[12] L. Escalera-Moreno, J. Baldoví, A. Gaita-Arino, and E. Coronado, Chem. Sci. **9**, 3265 (2018).
[13] W. H. Zurek, Rev. Mod. Phys. **75**, 715 (2003).
[14] L. Amico, R. Fazio, A. Osterloh, and V. Vedral, Rev. Mod. Phys. **80**, 517 (2008).
[15] P. Fazekas, *Lecture Notes on Electron Correlation and Magnetism* (World Scientific, Singapore, 1999).
[16] M. E. Fisher, Phys. Rev. **113**, 969 (1959).
[17] I. Syozi, *Phase Transition and Critical Phenomena* Vol. 1, edited by C. Domb, and M. S. Green (Academic Press, New York, 1972), pp. 269–329.
[18] O. Rojas, J. S. Valverde, and S. M. de Sousa, Physica A **388**, 1419 (2009).
[19] J. Strečka, Phys. Lett. A **374**, 3718 (2010).
[20] M. S. S. Pereira, F. A. B. F. de Moura, and M. L. Lyra, Phys. Rev. B **77**, 024402 (2008).
[21] M. S. S. Pereira, F. A. B. F. de Moura, and M. L. Lyra, Phys. Rev. B **79**, 054427 (2009).
[22] B. M. Lisnyi, Low Temp. Phys. **37**, 296 (2011).
[23] O. Rojas, S. M. de Souza, and N. S. Ananikian, Phys. Rev. E **85**, 061123 (2012).
[24] B. M. Lisnyi, Ukr. J. Phys. **58**, 195 (2013).
[25] M. Nalbandyan, H. Lazaryan, O. Rojas, S. M. de Souza, and N. Ananikian, J. Phys. Soc. Jpn. **83**, 074001 (2014).
[26] O. Rojas, S. M. de Souza, J. Torrico, L. M. Veríssimo, M. S. S. Pereira, and M. L. Lyra, Phys. Rev. E **103**, 042123 (2021).
[27] R. C. P. Carvalho, M. S. S. Pereira, M. L. Lyra, O. Rojas, and J. Strečka, Acta Phys. Polon. A **126**, 12 (2014).
[28] R. C. P. Carvalho, M. S. S. Pereira, I. N. de Oliveira, J. Strečka, and M. L. Lyra, J. Phys.: Condens. Matter **29**, 365801 (2017).
[29] H. S. Sousa, M. S. S. Pereira, I. N. de Oliveira, J. Strečka, and M. L. Lyra, Phys. Rev. E **97**, 052115 (2018).
[30] R. C. P. Carvalho, M. S. S. Pereira, I. N. de Oliveira, and M. L. Lyra, Physica A **526**, 121116 (2019).
[31] J. Čisárová and J. Strečka, Phys. Lett. A **378**, 2801 (2014).
[32] J. Čisárová and J. Strečka, Acta Phys. Pol. B **45**, 2093 (2014).
[33] J. Strečka and J. Čisárová, Mater. Res. Express **3**, 106103 (2016).
[34] L. Gálisová and J. Strečka, Phys. Rev. E **91**, 022134 (2015).
[35] L. Gálisová and J. Strečka, Acta Phys. Pol. A **127**, 216 (2015).

[36] L. Gálisová and J. Strečka, Phys. Lett. A **379**, 2474 (2015).
[37] L. Gálisová, Phys. Rev. E **96**, 052110 (2017).
[38] L. Gálisová and D. Jakubczyk, Physica A **466**, 30 (2017).
[39] L. Gálisová, Phys. B: Condens. Matter **536**, 498 (2018).
[40] J. Strečka, A. Tanaka, L. Čanová, and T. Verkholyak, Phys. Rev. B **80**, 174410 (2009).
[41] J. Strečka, A. Tanaka, and M. Jaščur, J. Phys.: Conf. Ser. **200**, 022059 (2010).
[42] L. Gálisová, J. Strečka, A. Tanaka, and T. Verkholyak, J. Phys.: Condens. Matter **23**, 175602 (2011).
[43] F. F. Doria, M. S. S. Perreira, and M. L. Lyra, J. Magn. Magn. Mater. **368**, 98 (2014).
[44] J. Strečka, H. Čenčariková, and M. L. Lyra, Phys. Lett. A **379**, 2915 (2015).
[45] H. Čenčariková, J. Strečka, and M. L. Lyra, J. Magn. Magn. Mater. **401**, 1106 (2016).
[46] H. Čenčariková, J. Strečka, and A. Gendiar, J. Magn. Magn. Mater. **452**, 512 (2018).
[47] H. Čenčariková and J. Strečka, Phys. Rev. E **98**, 062129 (2018).
[48] H. Čenčariková and J. Strečka, Phys. Lett. A **383**, 125957 (2019).
[49] H. Čenčariková, J. Strečka, and A. Gendiar, Physica E **115**, 113717 (2020).
[50] H. Čenčariková and J. Strečka, Physica A **566**, 125673 (2021).
[51] S. J. Gu, S. S. Deng, Y. Q. Li, and H. Q. Lin, Phys. Rev. Lett. **93**, 086402 (2004).
[52] S. S. Deng and S. J. Gu, Chin. Phys. Lett. **22**, 804 (2005).
[53] S. Hill and W. K. Wootters, Phys. Rev. Lett. **78**, 5022 (1997).
[54] W. K. Wootters, Phys. Rev. Lett. **80**, 2245 (1998).
[55] A. Rycerz, New. J. Phys. **19**, 053025 (2017).
[56] F. Souza, G. M. A. Almeida, M. L. Lyra, and M. S. S. Pereira, Phys. Rev. A **102**, 032421 (2020).
[57] M. Hase, H. Kitazawa, K. Ozawa, T. Hamasaki, H. Kuroe, and T. Sekine, J. Phys. Soc. Jpn. **77**, 034706 (2008).
[58] H. Kuroe, T. Hosaka, S. Hachiuma, T. Sekine, M. Hase, K. Oka, T. Ito, H. Eisaki, M. Fujisawa, S. Okubo, and H. Ohta, J. Phys. Soc. Jpn. **80**, 083705 (2011).
[59] M. Matsumoto, H. Kuroe, T. Sekine, and M. Hase, J. Phys. Soc. Jpn. **81**, 024711 (2012).
[60] S. Buhrandt and L. Fritz, Phys. Rev. B **90**, 094415 (2014).
[61] A. Otsuka, D. V. Konarev, R. N. Lyubovskaya, S. S. Khasanov, M. Maesato, Y. Yoshida, and G. Saito, Crystals **8**, 115 (2018).
[62] L. Onsager, Phys. Rev **65**, 117 (1944).
[63] C. Domb, Adv. Phys. **9**, 149 (1960).
[64] B. M. McCoy and T. T. Wu, *The Two-Dimensional Ising Model* (Harvard University Press, Cambridge, 1973).
[65] J. H. Barry, M. Kathun, and T. Tanaka, Phys. Rev. B **37**, 5193 (1988).
[66] M. Khathun, J. H. Barry, and T. Tanaka, Phys. Rev. B **42**, 4398 (1990).
[67] J. H. Barry, T. Tanaka, M. Khatun, and C. H. Múnera, Phys. Rev. B **44**, 2595 (1991).
[68] J. H. Barry and M. Khathun, Phys. Rev. B **51**, 5840 (1995).
[69] H. B. Callen, Phys. Lett. **4**, 161 (1963).
[70] M. Suzuki, Phys. Lett. **19**, 267 (1965).
[71] T. Balcerzak, J. Magn. Magn. Mater. **246**, 213 (2002).
[72] C. N. Yang, Phys. Rev. **85**, 808 (1952).
[73] J. Villain, Z. Phys. B **33**, 31 (1979).
[74] J. Villain, R. Bidaux, J.-P. Carton, and R. Conte, J. Phys. (Paris) **41**, 1263 (1980).
[75] V. M. Rozenbaum, Zh. Eksp. Teor. Fiz. **83**, 326 (1982) [Sov. Phys. JETP **56**, 178 (1982)].